

An analytic performance model for overlapping execution of memory-bound loop kernels on multicore CPUs

Ayesha Afzal, Georg Hager, Gerhard Wellein
 Department of High Performance Computing
 Erlangen Regional Computing Center
 Friedrich-Alexander-Universität Erlangen-Nürnberg, Germany
 {ayesha.afzal,georg.hager,gerhard.wellein}@fau.de

Abstract—Complex applications running on multicore processors show a rich performance phenomenology. The growing number of cores per ccNUMA domain complicates performance analysis of memory-bound code since system noise, load imbalance, or task-based programming models can lead to thread desynchronization. Hence, the simplifying assumption that all cores execute the same loop can not be upheld. Motivated by observations on plain and modified versions of the HPCG benchmark, we construct a performance model of execution of memory-bound loop kernels. It can predict the memory bandwidth share per kernel on a memory contention domain depending on the number of active cores and which other workload the kernel is paired with. The only code features required are the single-thread cache line access frequency per kernel, which is directly related to the single-thread memory bandwidth, and its saturated bandwidth. It can either be measured directly or predicted using the Execution-Cache-Memory (ECM) performance model. The computational intensity of the kernels and the detailed structure of the code is of no significance. We validate our model on Intel Broadwell, Intel Cascade Lake, and AMD Rome processors pairing various streaming and stencil kernels. The error in predicting the bandwidth share per kernel is less than 8%.

I. INTRODUCTION

With the number of cores and the peak performance of modern multicore chips still growing, the memory bandwidth bottleneck is becoming more severe. Many algorithms in computational science are based on building blocks that show memory-bound behavior, i.e., whose performance does not scale but saturate with respect to the number of active cores when running on a memory contention domain (usually a ccNUMA domain). Performance saturation due to bandwidth saturation should be regarded as a sign that a code is fast enough to address an architectural bottleneck, so it is not a bad thing in general. It also opens a clear optimization path via the reduction of data transfers.

Beyond the simple saturation pattern, however, memory-bound code exhibits other, more interesting phenomenology. As was shown in [2], bulk-synchronous barrier-free MPI programs can show *desynchronization* on a contention domain, i.e., processes move away from the initial lockstep state into a state where execution of loops kernels overlaps with communication or idleness, leading to automatic communication hiding. This can be provoked by a deliberate injection of delays, but it can

also occur automatically by natural system noise and small load imbalances.

Although it is often observed in programs that have a significant communication overhead, desynchronization is not limited to this scenario. In fact, barrier-free code (and also modern, task-based programming models) allows for concurrent execution of code with very different characteristics on a contention domain. In this paper we investigate a specific scenario: concurrent execution of two different loop kernels on n cores each. We construct a performance model that can describe accurately the memory bandwidth share that each kernel attains. The model is thus able to predict whether desynchronization of back-to-back parallel kernels and the ensuing overlap will speed up or slow down the execution of threads compared to a purely homogeneous execution. It can also predict if the mutual overlap will amplify or reduce the desynchronization effect.

This paper is organized as follows. The rest of this section covers related work and a motivational example (HPCG). In Sect. II we describe the experimental setup and methodology, and Sect. III defines code and performance metrics. The performance model is developed in IV and validated in Sect. V, where we also discuss the connection to desynchronization and close the loop to the initial HPCG example. We give a summary and an outlook to future work in Sect. VI.

A. Motivation and related work

This investigation is based on prior work by Afzal et al. [1, 3, 2], who studied idle wave propagation and computational wave formation in parallel programs on a phenomenological level. An analytic model of overlapping computational kernels and communication time on a contention domain was lacking, however. Alappat et al. [4] observed the consequences of desynchronization in the context of the well-known HPCG benchmark:¹ While validating their Roofline model for the MPI-parallel HPCG, they observed that the DDOT2 (dot product $s+=a[i]*b[i]$) kernels were in fact faster than what the local memory bandwidth would allow for. The authors attributed this to process desynchronization during the preceding sparse matrix-vector multiplication (SpMV) kernel

¹<https://www.hpcg-benchmark.org/>

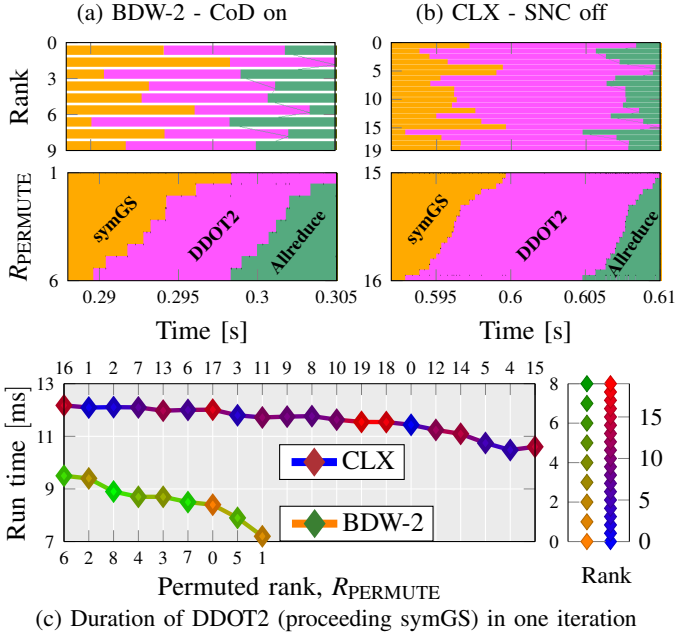


Fig. 1: MPI-only HPCG traces on one ccNUMA domain of Intel Broadwell (BDW-2) and Cascade Lake (CLX) at a problem size of 160^3 per process. Colors denote SymGS (orange), DDOT2 (pink), and MPI_Allreduce (green). Top panels in (a) and (b): timeline snippets from around a time stamp of 1628 s (x axes show offsets from this point). Bottom panels in (a) and (b): same data but with ranks sorted by the starting time of the DDOT2 kernel. (c) DDOT2 runtime per rank, same sorting as in bottom panels of (a) and (b).

and assumed that MPI processes that started the DDOT2 kernel early could benefit from immediate cache reuse, which was backed by a measured computational intensity that was higher than expected. However, it was unclear whether cache reuse was the only reason for the observed elevated DDOT2 performance.

The HPCG algorithm comprises the following kernels: six of BLAS-1 type (two DDOT2, one DDOT1 [$s += a[i] * a[i]$] and three DAXPY [$a[i] += s * b[i]$]) and one SpMV. Additionally, the multigrid preconditioner comprises five kernels: restriction, prolongation, SpMV, and two symmetric Gauss-Seidel routines (SymGS) as pre- and post-smoothers, each with a forward and a backward sweep, for coarsening and refinement.

HPCG has two types of MPI communication: a global collective operation (MPI_Allreduce) after each vector dot product and nonblocking point-to-point communication in SpMV and SymGS.

Figure 1(a) (top) shows a snippet from a timeline diagram of the HPCG benchmark (problem size 160^3 per process) on the nine cores of one ccNUMA domain of an Intel Broadwell processor (see Sect. II for hardware details and software setup). The colors encode the SymGS kernel (orange), the DDOT2 kernel (pink), and the MPI_Allreduce call (green). Note that this is only a part of a single iteration; all effects described here occur in every iteration of the algorithm.

The runtime of the SymGS kernel is about 20 times longer than that of DDOT2 here, so the clearly visible desynchronization effect has a minor influence on the SymGS performance. However, the execution of DDOT2 is strongly out of sync across processes. “Early” ranks still overlap with SymGS running on other cores, while “late” ranks overlap with waiting time (i.e., idleness) in MPI_Allreduce. The former must compete for memory bandwidth with SymGS and thus take longer to execute, while the latter can utilize more bandwidth per core, making them execute faster. This can be seen better in the lower part of Fig. 1(a), where we have sorted the MPI ranks according to the starting time of the DDOT2 kernel from early (bottom) to late (top). The late starters clearly take less time than the early starters, although the latter are those with cache reuse potential. In Fig. 1(b), the experiment was repeated on a 20-core Intel Cascade Lake processor. The effect is less pronounced here since the DDOT2 runtime is now significantly longer than the desynchronization time scale. There is hence less opportunity for DDOT2 to overlap with MPI_Allreduce.

Figure 1(c) shows the runtime of the DDOT2 kernel per rank in both experiments, using the same sorting as in (a) and (b). The runtimes are monotonically decreasing in both cases, showing clearly that late starters have better performance. In summary, the desynchronization of the SymGS kernel, in itself a negligible effect, leads to some cores executing the DDOT2 kernel faster due to overlapping with idleness in the MPI_Allreduce function. This is the real reason for the “faster-than-light” performance observed in [4].

In the broader context of desynchronized execution of barrier-free bulk-synchronous code, the general question arises how

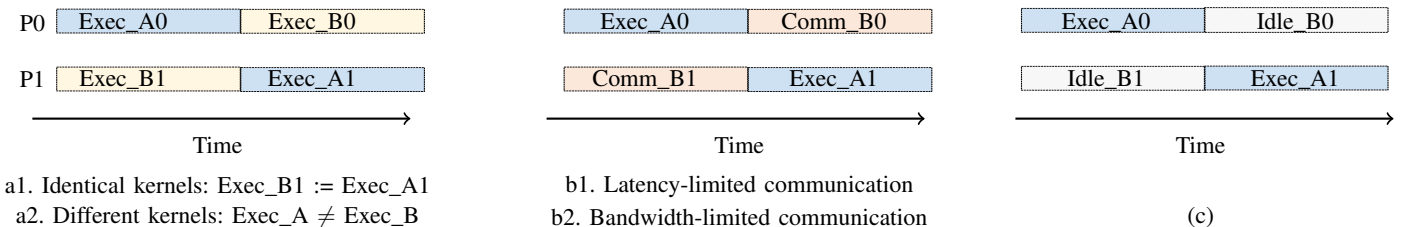
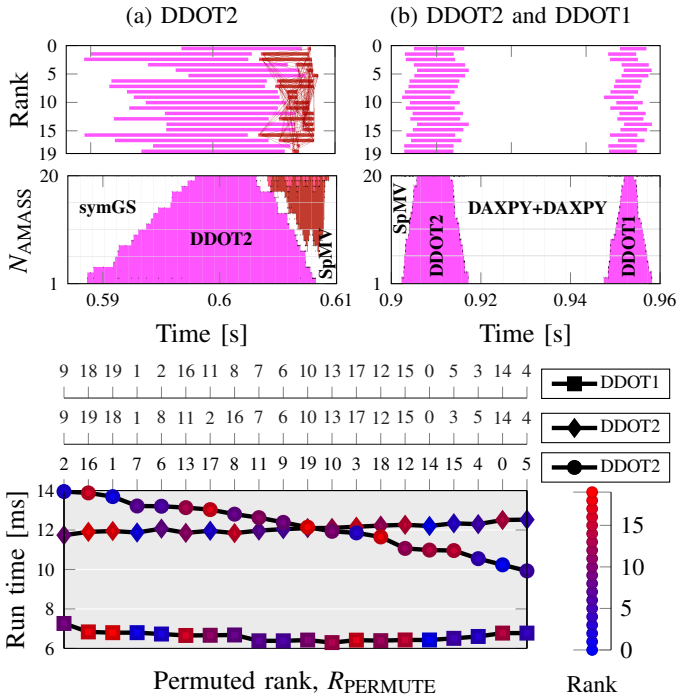


Fig. 2: Characterization of concurrency scenarios for bandwidth-limited computational kernels in parallel programs. “P0” and “P1” denote multi-threaded processes or groups of MPI processes within a contention domain. Each thread or process in a group executes the same code on different data. (a1, a2) Overlapping memory-bound loop kernels of different (or same) characteristics, (b1, b2) overlapping loop kernel execution with latency- or bandwidth-bound communication, and (c) overlapping loop kernel execution with idleness or code that addresses nonshared or scalable resources.



(c) DDOTx (proceeding symGS, SpMV and DAXPY) in one iteration

Fig. 3: Top panels of (a) and (b): Timeline snippets of a modified HPCG variant (missing any reduction operations) on an Intel CLX socket at a problem size of 160^3 per process, showing (a) DDOT2 between SymGS and SpMV and (b) DDOT2 and DDOT1 with two DAXPYs in between. The bottom panels of (a) and (b) show quantitative timelines of the number of ranks concurrently executing the DDOT kernels. Dark red color in (a) denotes time spent in `MPI_Wait` for nonblocking point-to-point communication during SpMVM. (c) shows time spent in the DDOTx kernels per core vs. permuted rank (permutation as in Fig. 1).

much bandwidth and thus performance can be achieved per core if different computational kernels are executed concurrently by cores on the same contention domain, if part of the cores are idle, or if they spend time communicating. Figure 2 shows the range of possible scenarios.

While scenario (b), i.e., overlapping of loop kernel execution with communication, was covered in [2], and scenario (c) is well described by the Execution-Cache-Memory performance model for multicore processors [7], scenario (a) was not studied before.

To further set the stage and motivate the relevance of the bandwidth sharing phenomenon, we conducted further experiments with a modified variant of HPCG that is identical to the original except for the lack of `MPI_Allreduce` calls. This allows for desynchronized states to survive for a long time, since no other global MPI operations are used in HPCG. We also executed a single iteration of the benchmark only. Figures 3 (a) and (b) shows timeline snippets of the modified HPCG on the same Intel Cascade Lake CPU as before. In Fig. 3(a) the DDOT2 kernel is sandwiched between a SymGS and an SpMV, while in Fig. 3(b) we show a broader view of

the two other DDOT kernels, with two DAXPY operations in between. As all global reductions were removed, the DDOTs are allowed to overlap with subsequent kernels.

In the bottom panels of (a) and (b) we show quantitative timelines that tell how many ranks execute the DDOT kernel at each point in time. This makes it easy to spot phases of homogeneous (i.e, single-kernel) execution and desynchronization. Qualitatively different behavior across the different DDOT kernels can be observed: In (a), where the tail end of the DDOT2 execution overlaps with a subsequent SpMV and its significant `MPI_Wait` time, the spread in endpoints of DDOT2 execution is smaller than the spread in their starting points. This is plausible because, as described earlier, early starters of DDOT2 take longer while late starters are faster. The effect can be quantified by a negative skewness parameter of the accumulated DDOT2 time distribution of -0.27 ms. The second DDOT2, however, is sandwiched between SpMV and DAXPY, so any overlap with idleness is ruled out. Instead, the interaction with the low-intensity DAXPY code seems to boost the desynchronization effect, i.e., the tail end of the accumulated DDOT2 time distribution is longer than the front end (skewness 0.42 ms). The last DDOT, which is actually a vector norm computation (DDOT1), shows a similar characteristic with an even larger positive skewness of 1.0 ms.

The skewness parameterizes the asymmetry in the distribution of a random variable, but the timeline data from the HPCG is not normally distributed even if the skewness is zero. However, we can use the skewness here to identify an important property of barrier-free parallel loop kernel execution: Negative skewness indicates *resynchronization*, while positive skewness indicates *desynchronization*. Which of the two occurs is obviously a function of which other workloads the kernel is embedded in. Note that the described effects in HPCG, even in our synchronization-free variant, are small in absolute numbers since the HPCG runtime is dominated by the multigrid and SpMV kernels. However, our observations open interesting questions towards the onset and mitigation of desynchronization effects in barrier-free memory-bound MPI programs. The goal of this paper is to establish a performance model for loop kernels of different characteristics running concurrently on a contention domain that can describe this scenario with sufficient accuracy. As an additional benefit, such a model can also predict the dynamics of task-based programming models on memory-bound code.

B. Contributions

This paper makes the following new contributions. (i) We identify the influence factors that govern the bandwidth share for individual threads in a “hybrid execution” setting, specifically two (groups of) threads running loops with different characteristics on a memory bandwidth contention domain: the “memory request fraction” to the memory interface and the saturated memory bandwidth of the different kernels. (ii) We employ ideas from the ECM performance model to predict the bandwidth share of different kernels on a contention domain. (iii) We validate the model for a set of 30 kernel pairings on four x86 architectures. Despite significant differences in hardware

TABLE I: Key hardware and software specifications of systems.

Systems	BDW-1	BDW-2	CLX	Rome
Processor	Broadwell EP	Broadwell EP	Cascade Lake SP	Zen
Model	Intel Xeon E5-2630 v4	Intel Xeon E5-2697 v4	Intel Xeon Gold 6248	ARM Epyc 7451
Base clock speed	2.2 GHz	2.3 GHz	2.5 GHz	2.35 GHz
Cores per NUMA domain (SMT)	10 (20)	18 (36)	20 (40)	8 (16)
Private L1 size	32 ($\times 10$) KiB	32 ($\times 18$) KiB	32 ($\times 20$) KiB	32 ($\times 8$) KiB
Private L2 size	256 ($\times 10$) KiB	256 ($\times 18$) KiB	1048 ($\times 20$) KiB	512 ($\times 8$) KiB
Shared LLC size	25 MiB (10 \times 2.5 MiB)	45 MiB (18 \times 2.5 MiB)	27.5 MiB (20 \times 1.375 MiB)	8 MiB (per 4 cores)
Memory per node (type)	64 GiB (DDR4)	384 GiB (DDR4)	128 GiB (DDR4)	128 GiB (DDR4)
LD/ST throughput (SIMD)	2/1 (AVX2/FMA3)	2/1 (AVX2/FMA3)	2/1 (AVX-512/FMA3)	2/1 (AVX2/FMA3)
L1 \rightleftharpoons L2 bandwidth	64 B/cy	64 B/cy	64 B/cy	32+32 B/cy
L2 \rightleftharpoons LLC bandwidth	32 B/cy	32 B/cy	16+16 B/cy	32 B/cy
LLC organization	Inclusive	Inclusive	Exclusive	Exclusive
Victim caches	No	No	LLC	LLC
El. transfers	Non-overlapping	Non-overlapping	Non-overlapping	Overlapping
Theor. MEM bandwidth	68.3 GB/s	76.8 GB/s	140.8 GB/s	170.6 GB/s
Compiler	Intel C++ v2019.5.281	Intel C++ v2019.5.281	Intel C++ v2019.5.281	Intel C++ v2019.5.281
Optimization flags (SIMD)	-O3 -xHost -xAVX	-O3 -xHost -xAVX	-O3 -qopt-zmm-usage=high -xCORE-AVX512	-O3 -xHost -mavx2
Message passing library	Intel MPI v2019u5	Intel MPI v2019u5	Intel MPI v2019u5	Intel MPI v2019u5
Operating system	CentOS Linux v7.7.1908	Ubuntu 18.04.3	Ubuntu 18.04.3	Ubuntu 18.04.3
ITAC	v2019u4	v2019u4	v2019u4	v2019u4
LIKWID	v5.0.1	v5.0.1	v5.0.1	v5.0.1

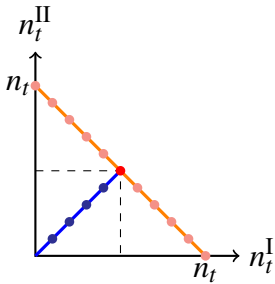


Fig. 4: Parameter space covered w.r.t. number of cores sharing a bottleneck (dots). n_t^I, n_t^{II} : number of cores running kernel I and II ; n_t : number of cores on ccNUMA domain. Orange: domain fully occupied; blue: symmetrical scaling.

properties across systems, the modeling error is below 8% globally and below 5% for 75% of cases.

Figure 4 visualizes the parameter space covered in this work with respect to numbers of threads sharing a contention domain. We only combine two distinct kernels, either filling the domain completely (orange dots) or scaling with equal core counts towards full saturation (blue dots). Other combinations were ignored for brevity although they can be described by the model just as well.

II. HARDWARE AND SOFTWARE SETUP, EXPERIMENTAL METHODOLOGY

To ensure the broad applicability of our results, we conducted all experiments on one ccNUMA domain of four different processors from Intel and AMD (see Table I for details on the hardware and software setup). Cluster-on-Die (CoD) and Sub-NUMA Clustering (SNC) were turned off on Intel CPUs (except for the experiments with HPCG on BDW in Sect. I-A), NPS4 mode (i.e., four ccNUMA domains per socket) was active on AMD Rome, and SMT threads were ignored, i.e., each application thread was assigned its own physical core. We always employed the widest SIMD instruction set supported by the architecture (AVX2 except on CLX where it was AVX-512)

and made sure that the compiler used standard (non-streaming) stores. The clock speed (core and uncore) was fixed to the base value via the `likwid-setFrequencies` tool from the LIKWID [9, 5] tool suite.

The transparent huge pages (THP) setting was put to “always,” and the NUMA balancing feature was turned off in order to reduce the performance impact from these settings [4]. All prefetching mechanisms in the hardware were enabled.

In order to run two groups of threads of different size and control thread-core affinity we used the `likwid-mpirun` tool. Working sets were chosen large enough to not fit into any cache (i.e., at least $10\times$ the last-level cache size), and data sharing across overlapping kernels was ruled out to eliminate the possibility of cache reuse.

Runtime traces were visualized using Intel trace analyzer and collector (ITAC)². All timings were taken using the C++ high-resolution `Chrono` clock. Individual kernel executions were repeated at least 15 times to even out variations in runtime. Memory bandwidths were measured by taking the ratio of data volume and wall-clock time.

The HPCG benchmark results presented in the introduction were obtained with version 3.1, a problem size of 160^3 (2.7GB per rank), and a configured runtime of 1800 seconds. In addition to the standard compiler flags, we used `-DHPCG_NO_OPENMP` for pure MPI, `-DHPCG_CONTIGUOUS_ARRAYS` for contiguous data layout, and `-trace -tcollect -tcollect-filter func.txt -qopt-report` to enable trace data collection and analysis of selected user functions (configured in `func.txt`).

Further details can be obtained from the example code we put up for download at <http://tiny.cc/ISPASS-OBS>.

²<https://software.intel.com/en-us/trace-analyzer>

TABLE II: Key specifications of computational kernels used in the experiments. All arrays and scalars hold double-precision floating point data. In all cases with write access, standard stores and write-back caches are assumed so that write-allocate transfers cannot be avoided. Note that data transfers and code balance pertain to the L3 cache for the stencil codes.

Cases	Naive Kernels	Pseudo-code for loop body	Elem. transf. (R+W+RFO)*	Code balance B_c [B/F]	Memory request fraction f				Saturated bandw. b_s [GB/s]			
					BDW-1	BDW-2	CLX	Rome	BDW-1	BDW-2	CLX	Rome
Read-only	vectorSUM	$s += a[i]$	1 (1+0+0)	8	0.241	0.178	0.125	0.590	59	66.9	111.1	34.7
	DDOT1	$s += a[i]*a[i]$	1 (1+0+0)	4	0.242	0.179	0.126	0.571	59	66.7	110.5	34.7
	DDOT2	$s += a[i]*b[i]$	2 (2+0+0)	8	0.252	0.181	0.142	0.665	56.5	65.8	108.7	33.6
	DDOT3	$s += a[i]*b[i]*c[i]$	3 (3+0+0)	8	0.255	0.181	0.166	0.721	56.8	65.5	100.9	33.1
Read-write	DSCAL	$a[i] = s * a[i]$	2 (1+1+0)	16	0.374	0.301	0.211	0.857	49.6	54.1	101.1	34.9
	DAXPY	$a[i] = a[i] + s * b[i]$	3 (2+1+0)	12	0.315	0.239	0.204	0.960	53.2	60.8	102.5	32.6
	ADD	$a[i] = b[i] + c[i]$	4 (2+1+1)	32	0.309	0.228	0.199	0.831	53.1	62.2	102	32.2
	STREAM	$a[i] = b[i] + s * c[i]$	4 (2+1+1)	16	0.309	0.228	0.199	0.838	53.2	62.2	102.4	32.2
	WAXPBY	$a[i] = r * b[i] + s * c[i]$	4 (2+1+1)	10.67	0.309	0.228	0.199	0.842	53.2	62.2	102.4	32.2
	DCOPY	$a[i] = b[i]$	3 (1+1+1)	24 [B/row]	0.320	0.242	0.190	0.803	53.5	60.9	104.2	32.5
	Schoenauer	$a[i] = b[i] + c[i] * d[i]$	5 (3+1+1)	20	0.299	0.223	0.185	0.859	53.1	60.5	101.7	31.7
	Jacobi-v1	§§										
	LC_{L2}	†	3 (1+1+1)	6	0.252	0.195	0.157	0.749	53.6	60.9	104.1	32.8
	LC_{L3}	‡	5 (3+1+1)	10	0.141	0.104	0.100	0.542	53.2	60.5	103.2	32.6
	Jacobi-v2	¶										
	LC_{L2}	†	4 (2+1+1)	2.46	0.247	0.188	0.167	0.804	53.5	62.3	102.9	33.2
LC_{L3}	‡	6 (4+1+1)	3.69	0.142	0.105	0.088	0.458	52.9	60.8	103.2	32.1	

* R: no. of read streams, W: no. of write streams, RFO: read-for-ownership (a.k.a. write allocate).

§§ Simple 2d 5-point stencil update: $b[j][i] = (a[j][i-1] + a[j][i+1] + a[j-1][i] + a[j+1][i]) * s$

† CL transfers and code balance in L3 for layer condition fulfilled at L2 (three data streams); grid size 20000×4000 (outer \times inner)

‡ CL transfers and code balance in L3 for violated layer condition at L2 (five data streams); grid size 5000×25000 (outer \times inner)

¶ More complicated 2d 5-point stencil update:

$r1 = (ax * (A[j][i-1] + A[j][i+1]) + ay * (A[j-1][i] + A[j+1][i]) + b1 * A[j][i] - F[j][i]) / b1$

$B[j][i] = A[j][i] - relax * r1$

residual $+= r1 * r1$

III. CODE AND PERFORMANCE METRICS

The *computational intensity* of a loop is the ratio of arithmetic operations (“true work,” e.g., flops) to the number of bytes that must be transferred over a data bottleneck in order to do the work. It is the main parameter that goes into the Roofline model [10], which assumes only two hardware bottlenecks: memory bandwidth and peak computational performance. Its inverse, the *code balance*, appears at first sight to be a reasonable metric to quantify the “hunger” of a loop for data. However, from the point of view of refined performance models such as the ECM model [8, 7], arithmetic instructions are an overlapping component of code execution. This means that the execution time of an executing loop does not depend on the actual number of flops but on the time spent moving data through the memory hierarchy unless the arithmetic work becomes dominant. The *performance* of the loop in flop/s does depend on the number of flops, however, but this is not the observable metric we are concerned with here.

We cannot give a full introduction to the ECM model here; instead, we describe the components that are relevant for our analysis on systems where the memory bandwidth is the sole data transfer bottleneck on a ccNUMA domain. The following contributions go into a single-core ECM runtime prediction:

- T_{OL} : In-core execution time of loop instructions that are not contributing to T_{L1Reg}

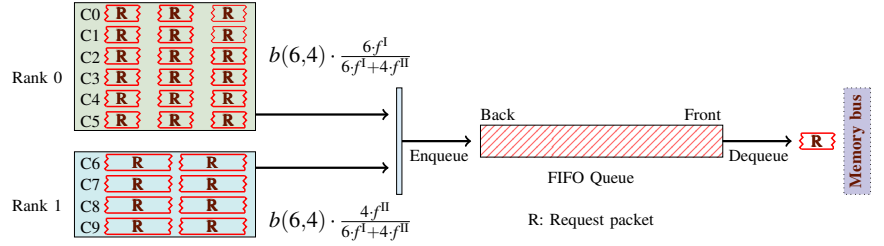
- T_{L1Reg} : Optimal execution time of all load and/or store instructions, assuming full pipeline throughput; i.e., minimum number of cycles required to retire these instructions
- T_{Mem} : Time for all required data transfers over the memory interface assuming that the full saturated memory bandwidth can be utilized
- $\{T_i\}$: Times for data transfers over all relevant data paths in the cache hierarchy, i.e., L2-L3 and L1-L2 in a three-level cache hierarchy

The ECM *machine model* makes assumptions about how these contributions have to be put together to arrive at a single-core runtime contribution. For example, on all Intel server CPUs to date, only loads count towards T_{L1Reg} , and the runtime is

$$T_{ECM} = \max \left(T_{OL}, T_{Mem} + \sum_{i=1}^n T_i + T_{L1Reg} \right), \quad (1)$$

i.e., data transfers are nonoverlapping while all instructions executed (except loads) in the core overlap with everything. The ECM *application model* provides information about the actual code (instructions and their dependencies) and data transfer volumes. It is usually obtained by static code analysis and assumptions about data transfers. In case of pure streaming loop kernels without temporal reuse, it is straightforward to calculate the data volumes. For stencils, a layer condition (LC) analysis [8] provides this information. The ECM model

Fig. 5: Basic model of memory bandwidth sharing. In the example, two kernels generate requests on six and four cores, respectively, and kernel II (on MPI rank 1) has a much higher $f^{\text{II}} \gg f^{\text{I}}$. It can queue more requests per core and thus get more share of bandwidth per core.



provides us with a resource-centric point of view on memory bandwidth utilization. The fraction of time the serial code occupies the memory interface is

$$f = \frac{T_{Mem}}{T_{ECM}}. \quad (2)$$

On a largely nonoverlapping memory hierarchy like in Intel server CPUs, the *memory request fraction* f is significantly smaller than one even for streaming kernels with no temporal locality; on AMD Rome, which has strongly overlapping characteristics, it is often close to one in this case. The value of f quantifies how much of the shared resource (the memory interface) can be utilized by a single core. In most memory-bound loops, f does not change if the number of flops (and hence the code balance) changes because the data transfers dominate in (1). This is why code balance is not a good metric for quantifying the need of a loop for data. In contrast to f , it does not take machine characteristics like the overlapping behavior of the cache hierarchy into account.

The value of f can be determined by using performance counters to measure the memory bandwidth drawn when executing a loop kernel in single-threaded mode. It can also be predicted by the analytic ECM model if the required knowledge about the hardware and code (see above) is available. We use the first option here and determine f per kernel as

$$f = \frac{b_{meas}}{b_s}, \quad (3)$$

where b_{meas} is the measured single-threaded memory bandwidth and b_s is the saturated (full-domain) memory bandwidth of the kernel.

The ECM model also predicts the scaling behavior of loops across cores on a contention domain. We use a simplified version of the recursive model presented in [6]. It assumes that, at n cores, a latency penalty of $p_0 \times u(n-1) \times (n-1)$ must be added, with $u(i)$ being the utilization of the memory interface at i cores, $u(1) = f$, and $p_0 = T_{Mem}/2$. This is not as accurate as the full model, in which p_0 is a fit parameter, but it will suffice for our purposes.

The maximum memory bandwidth b_s is not the same for all loop kernels. As a general rule on all x86 CPUs, read-only kernels achieve a somewhat (5%–15%) higher saturated bandwidth than kernels with write streams. While this effect is of minor importance in single-core modeling since the memory data transfer only accounts for a fraction (f) of the execution time at least on Intel CPUs, an accurate model of bandwidth sharing requires to take the differences in b_s into account.

Table II lists the loop kernels used for our experiments together with their basic properties such as number of elements

transferred over the memory interface per iteration (except for the stencils, where we show transfers to/from the L3 cache), their (memory or L3) code balance, their f values, and their saturated bandwidths. We include two 2d stencil algorithms with different characteristics. For each we select two different grid sizes that exhibit layer conditions (LC) fulfilled or broken at the L2 cache; if the LC is fulfilled, the data transfers between L3 and L2 are reduced because reuse across the outer stencil dimension is possible at the L2 cache. This happens when three consecutive rows of the source grid fit into L2. For the stencils we thus list the code balance in L3 instead of in memory, because the in-memory code balance is the same regardless of the LC at L2. However, the intra-cache data transfers between L2 and L3 make a significant difference for the memory request fraction f . See [8] for an in-depth coverage of layer conditions.

IV. ANALYTICAL MODEL

The central quantities in our bandwidth sharing model are the kernel's memory request fraction f and the saturated bandwidth b_s . As an example we look at a ten-core contention domain with six cores running kernel I (f^{I}) and four cores running kernel II (f^{II}) as depicted in Fig. 5. Each core issues requests at a certain fraction of the maximum rate; this fraction is f^{I} or f^{II} , respectively. In the model, this is also the rate at which requests are queued to be serviced by the memory interface. A kernel with higher f will be able to queue more requests. Since we are dealing with a fully populated contention domain, the requests from the ten cores compete for bandwidth, which is limited by a value that depends (though weakly) on the code characteristics. This variation is phenomenological input to the model. In Table II we listed the saturation bandwidths b_s for all kernels at homogeneous execution (no mixing). When two different kernels overlap, this value changes, and we assume that the overlapped saturated bandwidth is a weighted mean of homogeneous bandwidths:

$$b(n_t^{\text{I}}, n_t^{\text{II}}) = \frac{n_t^{\text{I}} \times b_s^{\text{I}} + n_t^{\text{II}} \times b_s^{\text{II}}}{n_t^{\text{I}} + n_t^{\text{II}}} \quad (4)$$

Here, b_s^{I} and b_s^{II} are the saturated bandwidths for the two kernels in homogeneous execution, and n_t^{I} and n_t^{II} are the respective numbers of threads, where $n_t = n_i^{\text{I}} + n_i^{\text{II}}$.

As shown in Fig. 5, where we chose $n_i^{\text{I}} = 6$ and $n_i^{\text{II}} = 4$, we now assume that group I of cores gets a share of all requests, and thus a share of the bandwidth, proportional to

$$\alpha^{\text{I}} = \frac{n_i^{\text{I}} \times f^{\text{I}}}{n_i^{\text{I}} \times f^{\text{I}} + n_i^{\text{II}} \times f^{\text{II}}} \quad \text{and} \quad \alpha^{\text{II}} = 1 - \alpha^{\text{I}}. \quad (5)$$

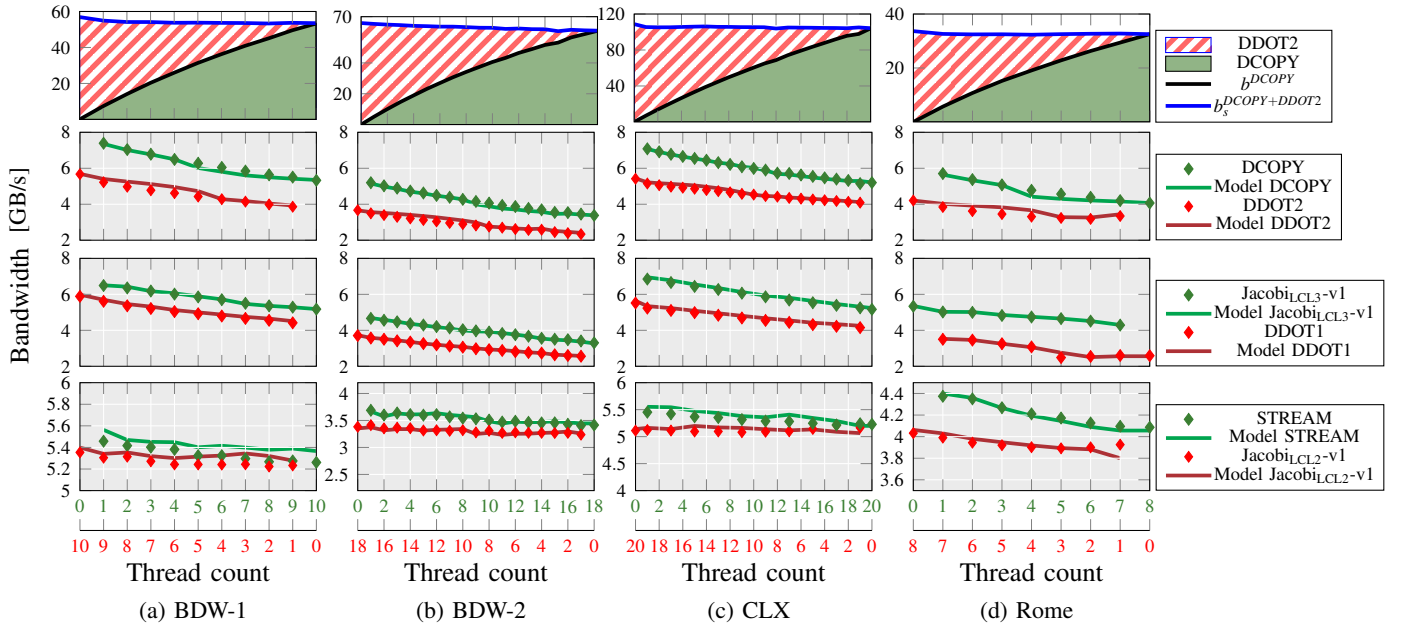


Fig. 6: Observed bandwidth per kernel vs. number of threads per kernel for the fully populated ccNUMA domain (thread parameter space: orange dots in Fig. 4) across all four architectures (columns (a)–(d)). Top row: Stacked graph of bandwidth share per kernel (DCOPY+DDOT2); the sum is the overall memory bandwidth (blue line). Second row: comparison of model (lines) with measurement (symbols) for the per-core memory bandwidth using the same pairing as above. Third and fourth row: same comparison for JacobiL3-v1+DDOT1 and STREAM+JacobiL2-v1, respectively.

In the homogeneous case $f^I = f^{II}$, the share of bandwidth is solely determined by the number of threads in each group, but different request fractions modify this simple linear behavior. The bandwidth obtained by group I is thus $\alpha^I \times b(n_r^I, n_r^{II})$.

This model, although we have derived it starting from the assumption that the ccNUMA domain is fully populated, can also be applied to the nonsaturated case. In the following section we will validate the model using measurements in the parameter space depicted in Fig. 4.

V. MODEL VALIDATION AND DISCUSSION

In this section we first present measurements of selected scenarios (i.e., kernel pairings) on the four architectures and compare with the model (5), distinguishing between the fully populated domain case and the case where the number of cores goes up till saturation. We then extend the view to more pairings and finally present an overview of the modeling error for all cases.

In Fig. 6 we show three different kernel pairing scenarios per architecture using fully populated ccNUMA domains (i.e., 10, 18, 20, and 8 cores on the four architectures (a)–(d)), covering the orange dots in Fig. 4. The top panel in each column shows a stacked graph of the bandwidth share of kernel I (DCOPY, green) versus kernel II (DDOT2, hatched red) as the number of threads on kernel I is increased and the number of threads on kernel II is reduced. The top line in the graph is the measured overall memory bandwidth. Since DCOPY has a higher f than DDOT2 (see Table II), we expect from the model (5) that DCOPY will get a higher share of the bandwidth as the number of DCOPY threads goes up. This is observed as the upward “bend” of the separator between the two regions of the graph. The overall memory bandwidth goes down because

the saturation bandwidth of DCOPY is smaller than that of DDOT2 (which is a read-only kernel that gets a little more bandwidth out of the memory interface). This behavior is quite universal across all four architectures for this kernel pairing.

The second panel in each column is a direct comparison between the modeled (lines) and observed (symbols) memory bandwidth per core for the DCOPY+DDOT2 case. Since we chose a zoomed-in y axis, the general downward trend stemming from the decline in saturated bandwidth is now more pronounced. Although not directly visible from the mathematical description, this change is just as important for the observed bandwidth as the difference in f . Obviously, the model describes the per-core bandwidth quite accurately.

The third and fourth panels in each column show per-core bandwidth for two other pairings: JacobiL3-v1+DDOT1 and STREAM+JacobiL2-v1. Especially in the latter case the saturated bandwidths of the two kernels are very similar, so the downward trend is weaker and also the bandwidth difference per core is smaller. Nevertheless the model also provides an accurate prediction here.

Figure 7 shows the same cases as above but for symmetrical thread scaling, running the same number of threads per kernel (blue dots in Fig. 4). There is good agreement between model and measurement along the bandwidth saturation curve as well, but some peculiarities are worth noting. The notable breakdown in bandwidth for DCOPY near saturation on BDW-1 is reminiscent of the overall scaling behavior of this kernel on this architecture, which shows a maximum bandwidth already before the domain is full. While the BDW CPUs and especially Rome show a rather strong decline in per-thread bandwidth already at two threads per kernel, CLX scales well from two to four, which reflects the fact that its single-core bandwidth is low

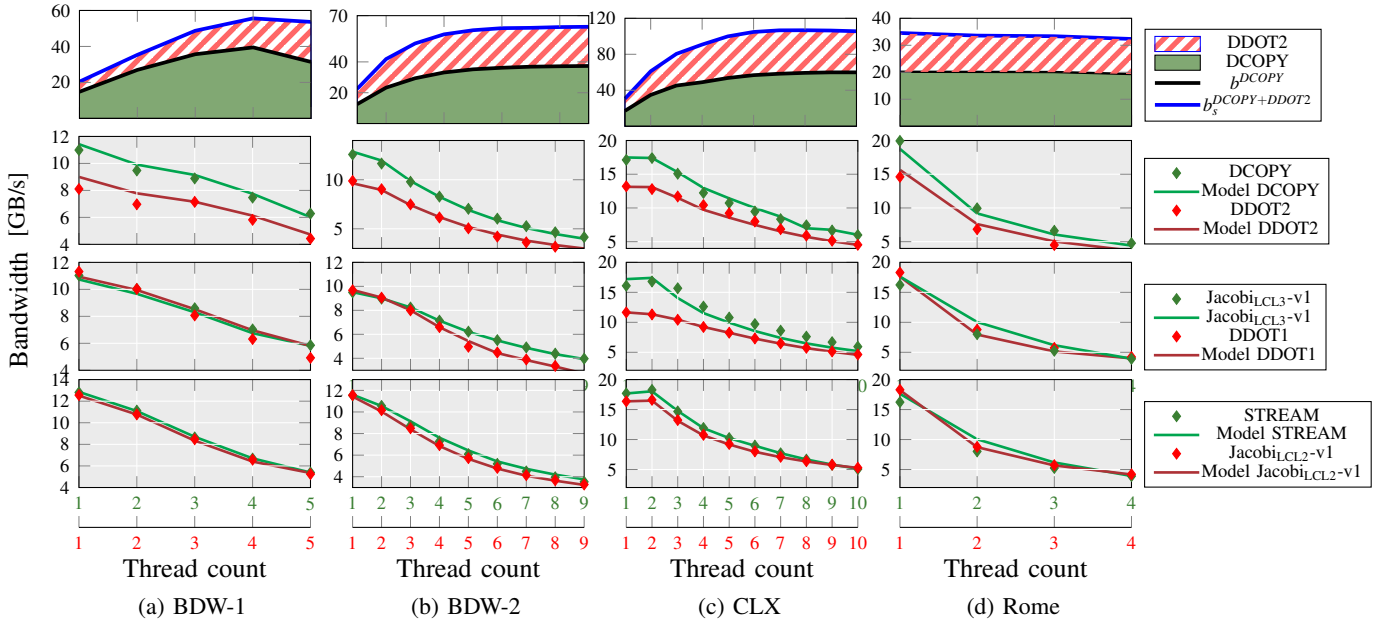


Fig. 7: Observed memory bandwidth per kernel vs. number of threads in symmetrical configuration, scaling across the ccNUMA domain (thread parameter space: blue dots in Fig. 4) for all architectures (columns (a)–(d)). Organization, kernels, and data plotted as in Fig. 6.

compared to its saturated bandwidth. Rome is special in terms of scaling since all kernels can almost saturate the memory bandwidth already with one thread due to its overlapping cache hierarchy. A more complete coverage of scaling results for more pairings can be found at <http://tiny.cc/ISPASS-OBS>.

In Fig. 8 we give a concise overview of the relative modeling error in per-core bandwidth across 30 kernel pairings along the bandwidth scaling curve, i.e., for symmetrical pairing. In 75% of all cases the error is below 5%, and the maximum overall error is 8%. In view of the significant differences in architectural details across the four CPUs (inclusive vs. victim LLC, shared vs. segmented LLC, overlapping vs. serializing caches) we consider this an exceptional result.

Figure 9 shows an overview of 32 kernel pairings (including self pairings) of vecSUM, DDOT2, DDOT3, DCOPY, Schoenauer, DAXPY, DSCAL, JacobiL2-v1, JacobiL3-v1, and TRIAD with others using an equal share of threads on a full contention domain. Each row of bars (a)–(d) refers to one architecture. Each bar represents the relative bandwidth share of

the first kernel in the pair (e.g., vecSUM in vecSUM+DDOT2) as opposed to the homogeneous situation (e.g., vecSUM paired with itself). All bars in a group are thus normalized to the first bar.

The first observation is that the patterns observed in each group of bars are quite consistent across architectures: Whether bandwidth is gained or lost with respect to the homogeneous situation depends on the ratio of f values of the kernels being greater or smaller than one. Across the Intel CPUs, this criterion is independent of the architecture. The CLX CPU is still special in the sense that the differences in bandwidth are smaller overall. One might be tempted to attribute this to the fact that it needs more cores to saturate the memory bandwidth than the BDW variants, i.e., it is “more scalable.” In other words, the memory transfers need less time relative to the other contributions in the single-core ECM model, which cause generally smaller request fractions f as can be seen in Table II. However, a global reduction factor in f cancels out in the model (5), hence this cannot be the reason for the weaker bandwidth variations. The

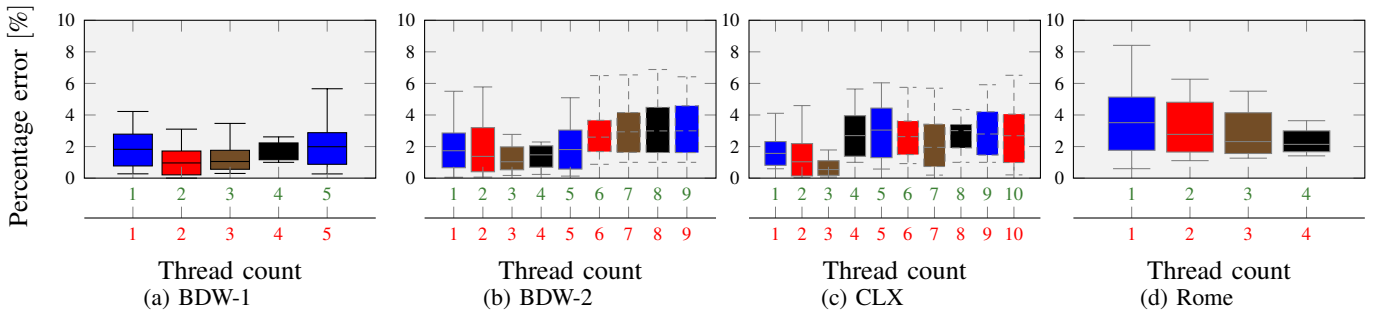


Fig. 8: Overview of modeling error across architectures (a)–(d) for symmetrical thread scaling (blue dots in Fig. 4) and 30 pairings per thread count and architecture. The error is calculated as $|(b_{\text{Observed}} - b_{\text{Model}})/b_{\text{Model}}|$. Whiskers denote min/max error, boxes encompass second and third quartiles, and the median is marked.

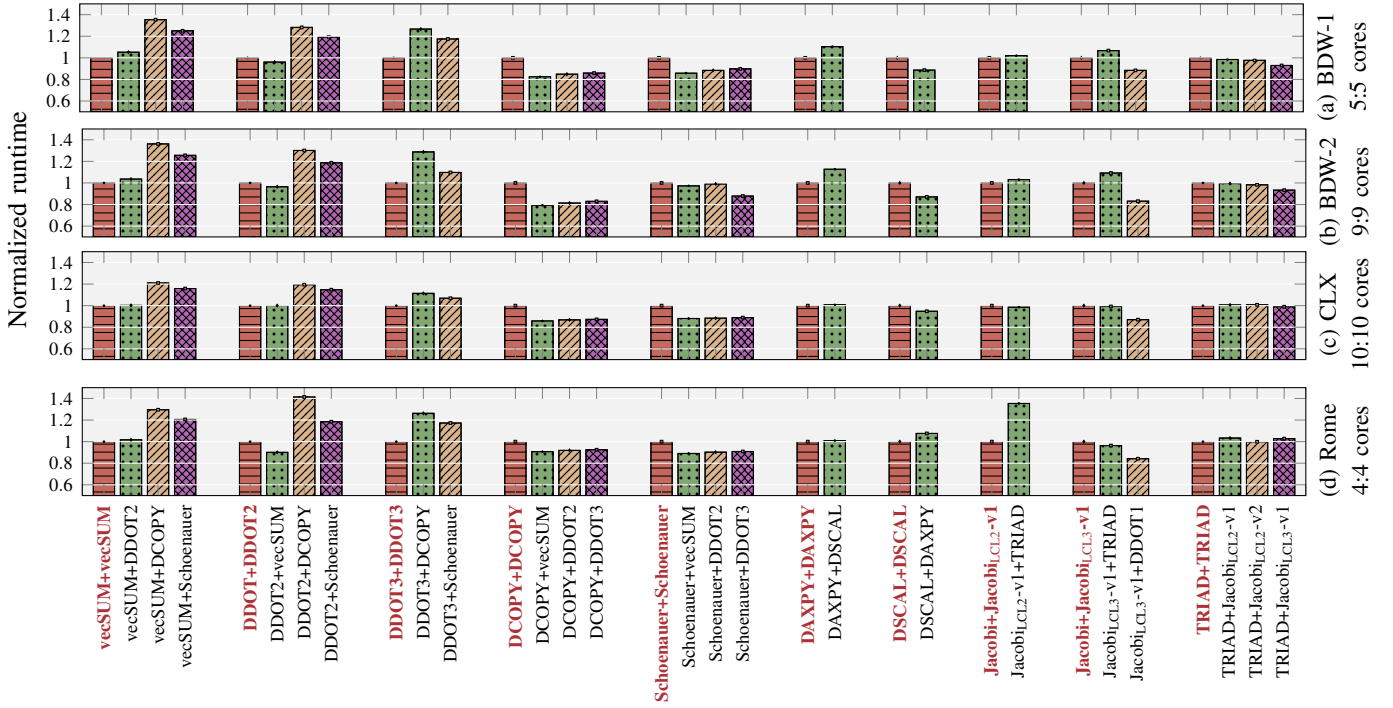


Fig. 9: Bandwidth gain or loss for symmetrical kernel pairings (each kernel gets half the contention domain) across architectures (a)–(d). The height of each bar is the relative gain or loss in bandwidth of the first kernel in the pair when paired with the second, normalized to the self-paired case (first bar in each group).

real reason for CLX showing smaller variations is two-fold: first, it shows less spread in saturated bandwidth than the other Intel CPUs across all kernels in Table II (10% as opposed to 20% for BDW-1); second, it also shows less spread in f values (2.4 vs. 2.7 for BDW-1). These two factors together lead to the reduced sensitivity of shared bandwidth to kernel variations on CLX. The AMD Rome CPU shows different patterns from the Intel chips for some combinations, especially for DAXPY+DSCAL. This due to $f^{\text{DAXPY}} > f^{\text{DSCAL}}$ on Rome as opposed to the Intel CPUs where this relation is reversed.

We started this discussion with a close look at plain and modified MPI-parallel HPCG variants (see Sect. I-A), where we observed how back-to-back compute kernels overlapping on a contention domain due to desynchronization could either lead to them slowing down or speeding up depending on the particular pairing. If a kernel is sandwiched between a high- f kernel coming before it and a low- f kernel coming after it, early starters get slowed down and late starters get sped up. This could be observed in Fig. 3(b), where the follow-up kernel to DDOT2 was DAXPY, with $f^{\text{DAXPY}} = 0.315$ and $f^{\text{DDOT2}} = 0.252$. This large difference directly leads to the positive observed skewness and means that the desynchronization is amplified in such a situation. Overlapping with idleness, as shown in Fig. 3(a) on the trailing edge of the DDOT2 execution, causes resynchronization. Our model is thus not only good for a quantitative description of performance differences on shared bottlenecks; it can also predict qualitatively the dynamics of desynchronization and resynchronization in memory-bound bulk-synchronous barrier-free programs.

VI. CONCLUSION AND OUTLOOK

Starting from observations of desynchronized kernel execution on the MPI-parallel HPCG benchmark we motivated the need for an analytical model of bandwidth sharing between groups of threads executing different loop kernels with different characteristics on a bandwidth contention domain. Based on the principles of the Execution-Cache-Memory (ECM) performance model, we constructed and validated such a model on four current x86 server processors from Intel and AMD. We could show that the major influence factors for bandwidth sharing between two groups of threads are each kernel’s memory request frequency, which is directly related to its single-threaded memory bandwidth, and its saturated bandwidth on the domain. Across a variety of pairings of kernels with and without cache reuse, the observed error in predicted per-core bandwidth was never larger than 8%, and lower than 5% for 75% of all cases. Apart from the quantification of bandwidth shares, the model is also able to predict how desynchronization across MPI processes gets amplified or mitigated depending on which back-to-back kernels are overlapped with each other in MPI-parallel barrier-free bulk-synchronous programs.

The set of loop kernels chosen here is a reasonable cross section with a spectrum of properties. Since the memory request fraction and the saturated memory bandwidth are the only relevant parameters in our model, it should be applicable also for more complex kernels (e.g., with more concurrent data streams or with dominant in-core execution). It should also be useful in modeling the performance of task-parallel code where the synchronized, data-parallel execution of threads may be

more the exception than the rule. A validation of the model on more processor architectures, e.g., Power- or Arm- based CPUs, is certainly in order. Finally, our work enables the development of a new kind of MPI simulation technique that can take node-level bottlenecks into account much more accurately than previously possible. We leave these investigations for future work.

ACKNOWLEDGMENTS

This work was supported by KONWIHR, the Bavarian Competence Network for Scientific High Performance Computing in Bavaria, under project name “OMI4papps.”

REFERENCES

- [1] A. Afzal, G. Hager, and G. Wellein. Delay flow mechanisms on clusters. URL: https://hpc.fau.de/files/2019/09/EuroMPI2019_AHW-Poster.pdf. Poster at EuroMPI 2019, September 10–13, 2019, Zurich, Switzerland.
- [2] A. Afzal, G. Hager, and G. Wellein. Desynchronization and wave pattern formation in MPI-parallel and hybrid memory-bound programs. In P. Sadayappan, B. L. Chamberlain, G. Juckeland, and H. Ltaief, editors, *High Performance Computing*, pages 391–411, Cham. Springer International Publishing, 2020. ISBN: 978-3-030-50743-5. DOI: [10.1007/978-3-030-50743-5_20](https://doi.org/10.1007/978-3-030-50743-5_20).
- [3] A. Afzal, G. Hager, and G. Wellein. Propagation and decay of injected one-off delays on clusters: A case study. In *2019 IEEE International Conference on Cluster Computing, CLUSTER 2019, Albuquerque, NM, USA, September 23-26, 2019*, pages 1–10, 2019. DOI: [10.1109/CLUSTER.2019.8890995](https://doi.org/10.1109/CLUSTER.2019.8890995).
- [4] C. L. Alappat et al. Understanding HPC benchmark performance on Intel Broadwell and Cascade Lake processors. In P. Sadayappan, B. L. Chamberlain, G. Juckeland, and H. Ltaief, editors, *High Performance Computing*, pages 412–433, Cham. Springer International Publishing, 2020. ISBN: 978-3-030-50743-5. DOI: https://doi.org/10.1007/978-3-030-50743-5_21.
- [5] J. Eitzinger and T. Röhl. LIKWID web pages. <https://github.com/RRZE-HPC/likwid>.
- [6] J. Hofmann, G. Hager, and D. Fey. On the accuracy and usefulness of analytic energy models for contemporary multicore processors. In R. Yokota, M. Weiland, D. Keyes, and C. Trinitis, editors, *High Performance Computing*, pages 22–43, Cham. Springer International Publishing, 2018. ISBN: 978-3-319-92040-5. DOI: [10.1007/978-3-319-92040-5_2](https://doi.org/10.1007/978-3-319-92040-5_2).
- [7] J. Hofmann et al. Bridging the architecture gap: abstracting performance-relevant properties of modern server processors. *Supercomputing Frontiers and Innovations*, 7(2), 2020. ISSN: 2313-8734. DOI: [10.14529/jsfi200204](https://doi.org/10.14529/jsfi200204).
- [8] H. Stengel, J. Treibig, G. Hager, and G. Wellein. Quantifying performance bottlenecks of stencil computations using the Execution-Cache-Memory model. In *Proceedings of the 29th ACM International Conference on Supercomputing, ICS '15, Newport Beach, CA. ACM, 2015*. DOI: [10.1145/2751205.2751240](https://doi.org/10.1145/2751205.2751240).
- [9] J. Treibig, G. Hager, and G. Wellein. LIKWID: a lightweight performance-oriented tool suite for x86 multicore environments. In *2012 41st International Conference on Parallel Processing Workshops*, pages 207–216, Los Alamitos, CA, USA. IEEE Computer Society, Sept. 2010. DOI: [10.1109/ICPPW.2010.38](https://doi.org/10.1109/ICPPW.2010.38).
- [10] S. Williams, A. Waterman, and D. Patterson. Roofline: an insightful visual performance model for multicore architectures. *Commun. ACM*, 52(4):65–76, 2009. ISSN: 0001-0782. DOI: [10.1145/1498765.1498785](https://doi.org/10.1145/1498765.1498785).